

Interferometric investigation of photonic band-structure effects in pure and doped colloidal crystals

Björn T. Rosner, Garrett J. Schneider, and George H. Watson

Department of Physics and Astronomy, University of Delaware, Newark, Delaware 19716

Received April 29, 1998; revised manuscript received August 11, 1998

A Mach-Zehnder interferometer was developed for accurately measuring relative phase shifts of light propagating in photonic colloidal crystals deep into the stop bands. These phase shifts can be used to determine the change in index of refraction and the optical dispersion relation from photonic band structure near the band edges. Phase measurements of colloidal crystals incorporating an impurity peak in the transmission spectrum are also presented. © 1998 Optical Society of America [S0740-3224(98)01211-9]

OCIS codes: 030.1670, 050.5080, 350.2460, 290.3030.

1. INTRODUCTION

Photonic bandgap structures are to photons what semiconductor crystals are to electrons. Photonic bandgap structures are fabricated by assembling three-dimensionally periodic structures, where the dielectric constants of the constituent media are different. Selection of the right materials and structure can yield complete photonic bandgaps, where the stop bands created by Bragg diffraction overlap for all directions and polarizations over a range of frequencies. Transmission and generation of electromagnetic waves in a certain wavelength range become prohibited in materials with complete bandgaps.¹⁻⁵ Complete two-dimensional photonic bandgaps in the visible and near-infrared regime have already been fabricated.⁶⁻⁸ These two-dimensional band-structure materials can be used to produce more efficient waveguides^{9,10} and microcavities.^{11,12} Three-dimensional photonic bandgaps in the optical regime have also been investigated experimentally and theoretically,¹³⁻¹⁶ but combining submicron feature sizes with macroscopic crystal dimensions has remained a challenge.

In this paper we report the dispersion relation of a photonic crystal measured by means of phase information acquired through interferometry. The photonic crystals considered here are three-dimensional arrays of polystyrene colloidal particles grown in an aqueous solution.^{17,18} Depending on volume fraction and particle diameter, the colloidal microspheres crystallize in either *bcc* or *fcc* structure. Photonic stop-band properties of both structures have been studied extensively.¹⁹⁻²¹ It has been shown theoretically²² that polystyrene colloidal crystals are not expected to exhibit a complete photonic bandgap because the lattice type is not ideal and the dielectric contrast between the low and the high dielectric regions is not adequate. However, colloidal crystals do permit studies of photonic band-structure effects and acquisition of the dispersion relation, as reported here.

The polystyrene microspheres have a permanent net negative charge on their surface, counterbalanced by free

ions in the solution. Since these colloidal crystals are formed without mechanical contact of the spheres, the screening length of the electrostatic interaction owing to the surface charge has to be increased until the interaction is strong enough to form a crystal lattice. This can be done by removing most of the stray ions. By use of ion-exchange resin the colloidal solution can be cleaned sufficiently to allow colloidal crystal growth.

Photonic crystals have been grown for this work from a colloidal suspension of polystyrene microspheres having a diameter of 0.173 μm and monodispersivity to within 3.1%.²³ The stock solution of 10% volume fraction was diluted to the desired volume fraction for an *fcc* crystal lattice. Since the (111) planes are the closest packed planes in the *fcc* structure, these planes naturally orient along the crystal cell window. When illuminating this crystal cell at normal incidence, the illumination is thus along the [111] direction. Kossel-line analysis²⁴ was used for examination of crystal quality and confirmation of the orientation.

A transmission spectrum of one of these crystals is shown in Fig. 1. The stop band of this *fcc* crystal along the [111] direction has its center wavelength λ_c at 890 nm and is about three orders of magnitude deep. The lattice spacing between adjacent (111) planes d_{111} is given by $d_{111} = m\lambda_c/2n$, which yields 0.330 μm , assuming first-order diffraction ($m = 1$) and an average index of refraction of $n = 1.35$, calculated with the Cauchy relations²⁵⁻²⁷ and 7% volume fraction. The decrease in transmission on the shorter wavelength side of the stop band shown in Fig. 1 arises from increased absorption and scattering from imperfections.

2. INTERFEROMETER DESIGN

Our experimental setup, shown in Fig. 2, consists of an Ar^+ ion laser pumping either an R6G dye laser or a Ti:Sa laser, with tuning ranges of 570–640 nm and 700–1010 nm, respectively. The Ti:Sa laser's wide tuning range

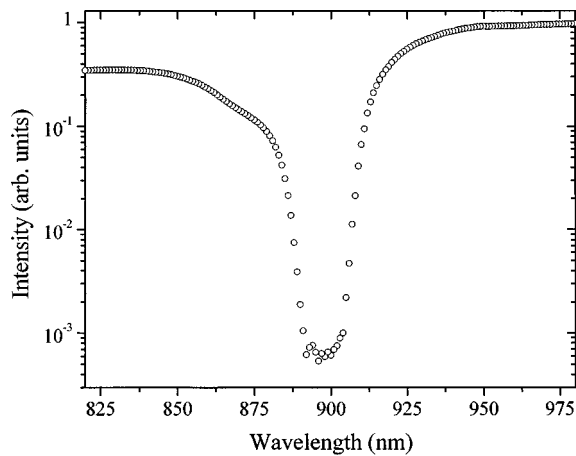


Fig. 1. Transmission spectrum along the *fcc* [111] direction of a colloidal crystal made of polystyrene microspheres and water, with 0.173- μm -diameter particles and 7% volume fraction.

makes it possible to measure phase shifts far outside the stop band, enabling a more accurate determination of the free-photon limit. Only data acquired with the Ti:Sa laser shall be discussed in detail here; previous measurements taken with the dye laser are included for comparison.²⁸

A modified Mach-Zehnder interferometer,²⁹ shown in Fig. 3, was chosen for this work because of its orthogonality of adjustments. Pinholes on the empty cell and the crystal cell were used to scan only a small section of the colloidal crystal at a time. The fringe patterns in the interferometer were captured by a CCD camera for each step in wavelength, as shown in Fig. 4. A nonlinear least-squares fit of Eq. (1) to each fringe pattern was used to extract the desired phase information:

$$I = I_{\text{avg}} \exp \left[- \left(\frac{x - \mu}{w} \right)^2 \right] [1 + \mathcal{V} \cos(2\pi f x + \Delta\Phi)]. \quad (1)$$

Here, I_{avg} is the intensity, and μ and w are the center position and the width, respectively, of the Gaussian envelope. The spatial frequency and the phase of the fringe pattern are f and $\Delta\Phi$, respectively. \mathcal{V} is the visibility of the fringe pattern, defined as the difference between the minimum and maximum intensities relative to I_{avg} ; it is a measure of the contrast in the fringe pattern.

Variable neutral attenuation wheels, AW_1 – AW_3 in Fig. 3, were used to change overall intensity and to maintain high fringe visibility as the wavelength was tuned to the stop-band center. The effect of these adjustments may be seen in Fig. 5, which shows that the visibility can be maintained at a high value of >0.5 until the transmission through the sample drops by over two orders of magnitude. Fringe movement arising from the repositioning of the attenuation wheels was automatically removed by the data-acquisition program. For Fig. 5 a thin-film interference notch filter was used as a reference sample.³⁰

The entire tuning range of the Ti:Sa laser can be explored by use of three different output couplers; however, the output direction and the position of the laser beam changes slightly after changing and realigning the mirror sets. Since it is important to maintain the same path

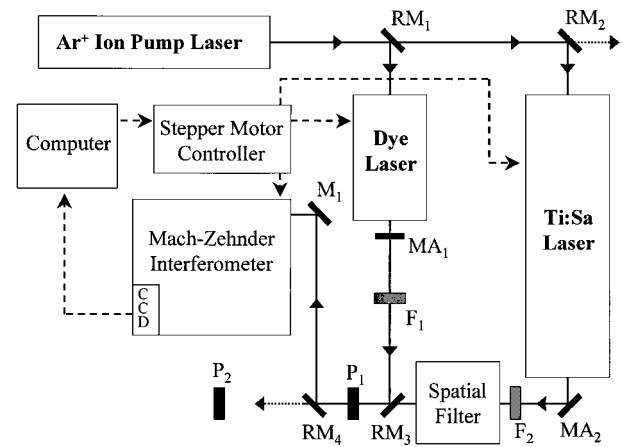


Fig. 2. Experimental setup for gathering phase information with a dye laser or a Ti:Sa laser as tunable laser sources. F_1 and F_2 are neutral-density filters, RM_1 – RM_4 are removable mirrors, MA_1 and MA_2 are mirror assemblies for beam steering, and P_1 and P_2 are pinholes for alignment purposes. Solid lines indicate laser beam paths, while dashed lines show the data flow.

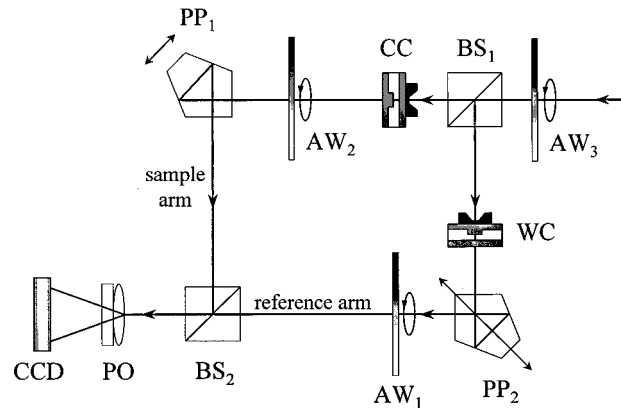


Fig. 3. Modified Mach-Zehnder interferometer. The fringe pattern is positioned in front of the CCD camera by adjustment of pentaprism PP_1 . The optical paths are equalized by adjustment of pentaprism PP_2 along a line perpendicular to PP_1 . The relative intensity in the reference arm is optimized for maximum fringe visibility before and during the scan via the neutral attenuation wheels AW_1 – AW_3 . The cell WC contains water, while the crystal cell CC contains the photonic crystal. PO, polarizer and objective; BS, beam splitter.

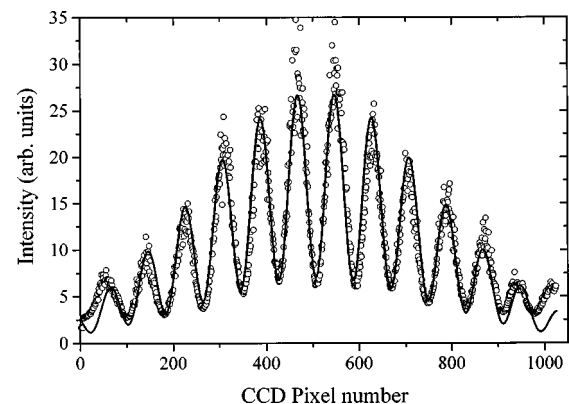


Fig. 4. Typical interferometer fringe pattern with optimized fringe visibility $\mathcal{V} = 0.59$. The solid curve is the resulting nonlinear least-squares fit of Eq. (1).

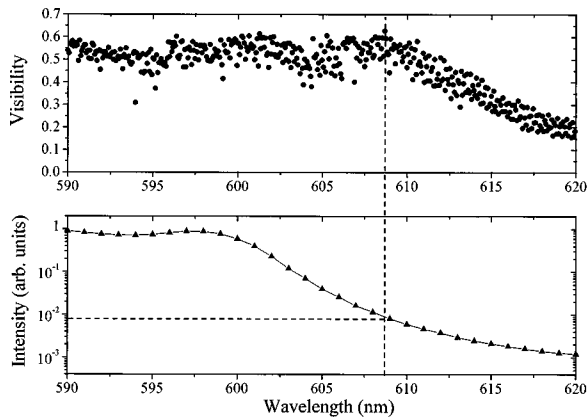


Fig. 5. Effect of the attenuation wheels AW_1 and AW_2 . The top plot shows the visibility of the fringe pattern in comparison with the lower plot, which shows a transmission scan through the reference sample used. It can be observed that the visibility stays at a high value of 0.5–0.6 up to 2.5 orders of magnitude into the stop band.

lengths in each arm of the interferometer, it was necessary to steer the Ti:Sa laser output in a reproducible way. A spatial filter and a mirror assembly, MA_2 , were used. Maximizing the output behind the spatial filter by moving the beam horizontally and vertically as well as tilting it before entering the spatial filter yielded a reproducible beam direction, enabling interferometry with all mirror sets in one data set.

3. REMOVING BACKGROUND PHASE SHIFT

Dispersion arising from the optical elements in the interferometer was almost completely removed by careful selection of matching elements in each arm. Each optical element in one arm had a counterpart of equivalent dispersion in the other arm. The optical path lengths inside the interferometer were equalized as accurately as possible with the sample present. This was accomplished by minimizing the fringe movement as the wavelength was tuned over a small range far outside the stop band. Since the path difference can be minimized but not completely removed, there is a residual phase shift when the wavelength is tuned that does not arise from the photonic band structure. Figure 6 shows this phase shift in multiple scans taken with no sample cells present, when all mirror sets of the Ti:Sa laser are used and the entire tuning range is covered. It can be seen that the different scans line up very well, indicating that the beam position and the direction following the spatial filter were reproducible with a change of the output coupler. With the wider tuning range of the Ti:Sa laser it can also be seen that this phase shift is not linear in the wavelength, as had been assumed previously for a smaller tuning range.²⁸ A model for the wavelength dependence of this nonphotonic phase shift observed in the fringe pattern is presented below.

The phase difference $\Delta\phi_1$ between the two beams at a reference wavelength λ_{v1} is related to the path difference by

$$\frac{\Delta\phi_1}{2\pi} = \frac{\Delta x}{\lambda_{v1}}, \quad (2)$$

where Δx is the optical path difference between the two arms. The subscript v denotes that the vacuum wavelength is used in the following equations. Similarly, the phase difference $\Delta\phi_2$ for any other wavelength λ_{v2} can be expressed as

$$\frac{\Delta\phi_2}{2\pi} = \frac{\Delta x}{\lambda_{v2}}. \quad (3)$$

The difference between these two phase differences is equal to the fringe movement at the CCD camera,

$$\frac{\Delta\phi_0}{2\pi} = \frac{\Delta\phi_1 - \Delta\phi_2}{2\pi} = \Delta x \left(\frac{1}{\lambda_{v1}} - \frac{1}{\lambda_{v2}} \right). \quad (4)$$

The phase difference $\Delta\phi_0$ is measured with respect to the fringe pattern at the reference wavelength λ_{v1} , i.e.,

$$\Delta\phi_0(\lambda_{v1}) \equiv 0. \quad (5)$$

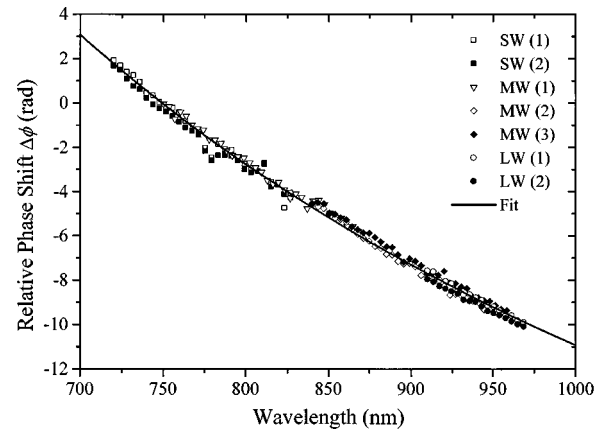


Fig. 6. Phase shift without a photonic crystal. Owing to slightly unequal optical path lengths, a phase shift is introduced as the wavelength is changed. This graph shows multiple scans with all three mirror sets of the Ti:Sa laser spanning the entire wavelength range. The number of data points was reduced for clarity. The line is a least-squares fit of Eq. (4).

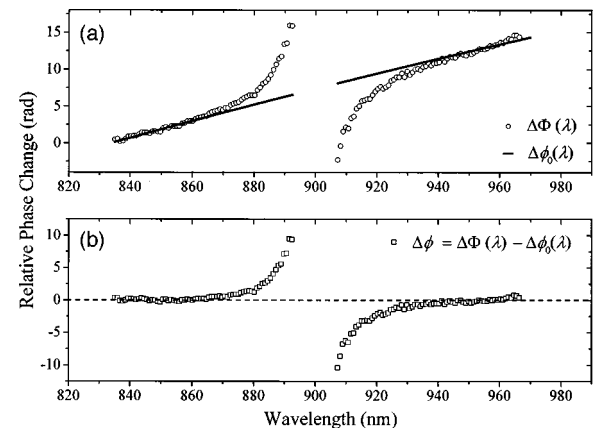


Fig. 7. Raw data $\Delta\Phi(\lambda)$ and the best fit of the fit function $\Delta\phi_0(\lambda)$ are shown in part (a). Subtracting the fitted phase from the raw phase data gives the phase-shift difference $\Delta\phi$ in (b) arising solely from the photonic stop band. Far away from the stop band, the free-photon limit is approached.

It is also possible to include the effect of normal dispersion in the cell with colloidal suspension and the water cell by splitting Δx in two parts,

$$\Delta x(\lambda_v) = \Delta x_{\text{phys}} + \Delta x_{\text{disp}}(\lambda_v). \quad (6)$$

Here, Δx_{phys} is the optical path difference between the two interferometer arms at the reference wavelength λ_{v1} , and $\Delta x_{\text{disp}}(\lambda_v)$ is the additional optical path difference introduced by normal dispersion in the water and the sample cell when the wavelength is tuned. For numerical purposes this means that a nonlinear least-squares fit to Eq. (4) may be applied with the parameters λ_{v1} and Δx_{phys} . For the data shown in Fig. 6, Δx_{phys} was $5.2 \mu\text{m}$ according to the result of the fitting procedure. The fitted $\Delta\phi_0$ may be subtracted from the raw phase data $\Delta\Phi$, leaving the phase change arising solely from the photonic structure, $\Delta\phi(\lambda_v)$,

$$\Delta\phi(\lambda_v) = \Delta\Phi(\lambda_v) - \Delta\phi_0(\lambda_v). \quad (7)$$

The result of this procedure is shown in Fig. 7 for the colloidal crystal discussed earlier. Far away from the stop-band edge in the free-photon limit, the phase change approaches zero on both sides.

4. DEVIATION OF INDEX OF REFRACTION

The observed phase shift $\Delta\phi(\lambda_v)$ may be related to an anomalous deviation in the index of refraction. In the conversion presented below, the index of refraction and the wave vector are assumed to be real quantities; this conversion is approximate given that the wave vector becomes complex within the stop band. However, for the polystyrene colloidal crystals studied here this has been shown to be an excellent approximation, where the imaginary portion of the wave vector remains less than 1% of the magnitude across the stop band.³¹ For systems with stronger scattering or a larger effective index of refraction the conversion process should incorporate complex quantities.

The total index of refraction of the crystal, $n_c(\lambda_v)$, may be split into a “normal” index $n_{c0}(\lambda_v)$ and a deviation part, $\Delta n_c(\lambda_v)$,

$$n_c(\lambda_v) = n_{c0}(\lambda_v) + \Delta n_c(\lambda_v), \quad (8)$$

where $\Delta n_c(\lambda_v)$ is related to $\Delta\phi(\lambda_v)$ by

$$\Delta n_c(\lambda_v) = \frac{\Delta\phi(\lambda_v)}{2\pi} \frac{\lambda_v}{d_{\text{sample}}}. \quad (9)$$

The thickness of the sample, d_{sample} , was determined to be $600 \mu\text{m} \pm 20 \mu\text{m}$. The resulting $\Delta n_c(\lambda_v)$ may be seen in Fig. 8. It should be mentioned that the sign of $\Delta n_c(\lambda_v)$ is undefined because the direction of phase shift is determined by the interferometer setup, not the photonic material itself. Hence one must assign the correct sign to $\Delta n_c(\lambda_v)$ by observing the direction of curvature of the dispersion relation. The resulting deviation $\Delta n_c \approx \pm 0.0025$ at the band edges is clearly evident and is expected to grow as the center of the stop band is approached.

When the stop band is entered, the signal-to-noise ratio decreases because the transmitted intensity through the crystal decreases by orders of magnitude, while the trans-

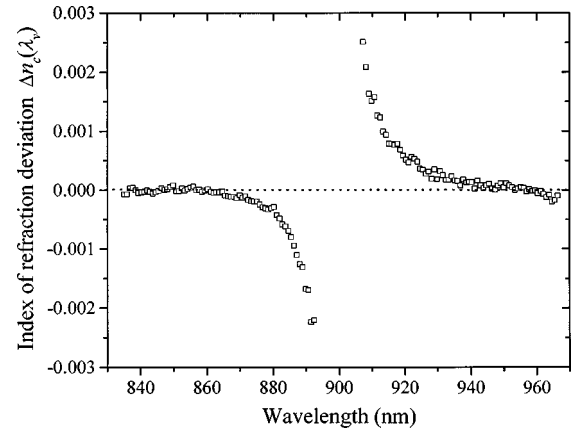


Fig. 8. Deviation of the index of refraction near the stop band, calculated from the phase data in Fig. 7(b) with Eq. (9). The phase information is lost when the stop-band center is approached because of a strongly decreased signal-to-noise ratio.

mitted intensity through imperfections and inclusions, which is not related to the dispersion relation of the photonic crystal, stays constant. Deep inside the stop band, the fringe patterns become noisier and fitting the phase change becomes less accurate; hence a gap appears in the relative phase and the refractive index reported.

For determining the direction of $\Delta\phi(\lambda_v)$, the experimental data may be compared with a theoretical prediction for the dispersion relation.³² The dispersion relation may be determined as follows. By definition,

$$\frac{2\pi}{k} = \lambda = \frac{\lambda_v}{n_c(\lambda_v)}. \quad (10)$$

With Eqs. (8) and (9) for n_c , the dispersion relation can be written as

$$k(\omega) = \frac{\omega}{c} + \frac{\Delta\phi(\omega)}{d_{\text{sample}}}. \quad (11)$$

5. PHASE MEASUREMENTS WITH DOPED CRYSTALS

Microwave models have already demonstrated that sharp transmission peaks may be introduced inside the stop band by intentional introduction of defects in an otherwise perfect photonic crystal.³³ In the case of colloidal crystals it is possible to substitute a small amount of colloidal microspheres with particles of a slightly different size. Transmission scans of the resulting crystals have been studied previously.³⁴ A transmission scan along the [111] direction of such a crystal is shown in Fig. 9; this particular crystal consists of $0.173\text{-}\mu\text{m}$ polystyrene host particles with 7% of the host particles replaced by $0.203\text{-}\mu\text{m}$ polystyrene impurity particles. The impurity peak has a height of ~ 1.5 orders of magnitude above the stop-band transmission minimum.

The interferometric data, shown in Fig. 10, were taken in multiple scans with the Ti:Sa laser using both the medium-wave and the long-wave output couplers. The transmission scan from Fig. 9 is superimposed on the phase data to show the correspondence between the various features in the two data sets. The diverging phase at

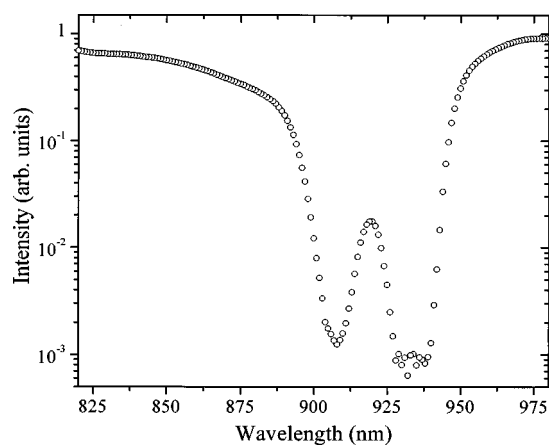


Fig. 9. Transmission spectrum along the *fcc* [111] direction of a doped photonic crystal. The impurity peak is located at 920 nm with an intensity of one order of magnitude above the stop-band transmission minimum. The colloidal crystal consists of 0.173- μm polystyrene host particles with 7% of the host particles replaced with 0.203- μm impurity particles.

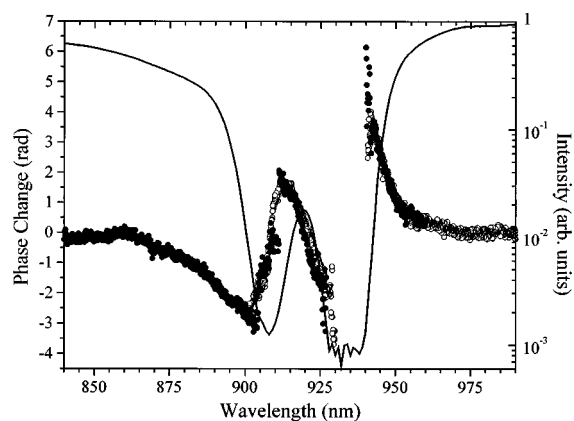


Fig. 10. Phase change (circles) and transmission curve (line) of a doped colloidal photonic crystal. The phase data were acquired with the medium-wave output coupler (black circles) and the long-wave output coupler (open circles).

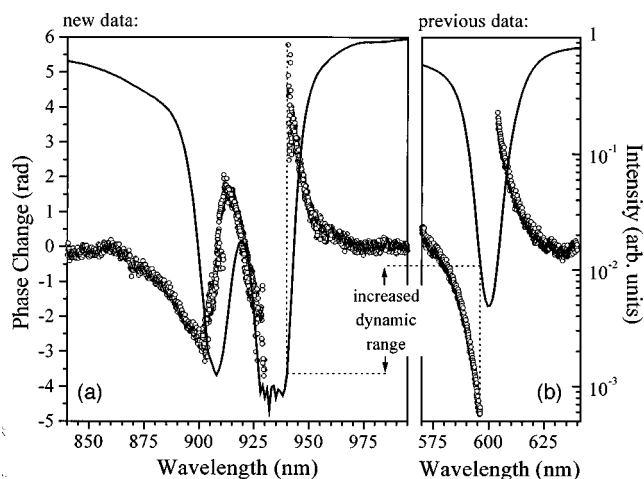


Fig. 11. Data from Fig. 10, shown in (a), compared with previously acquired data²⁸ in (b). The wide tuning range and the high dynamic range of the improved instrument are necessary to obtain the free-photon limit and the phase data of the impurity peak, respectively. For ease of comparison, all axes have the same scaling.

the long-wavelength side of the stop band is evident, as for the case of pure colloidal crystals. However, there is a feature at the lower-wavelength side that is not present in the phase change from a pure crystal. The apparent maximum in phase change at 912 nm is related to the appearance of the impurity peak in the transmission scan. It also appears that features in the phase data such as extrema and wavelengths of divergence are taking place where the transmission curve has inflection points.

Figure 11 shows a comparison of previously published phase and transmission data acquired from a pure colloidal crystal²⁸ and data recently acquired from the doped colloidal crystal. For ease of comparison the two graphs have the same scaling on all axes. When the transmission curves are compared, it is clear that the doped crystal has a much wider stop band than the pure crystal. The stop band is about as wide (60 nm) as the entire tuning range of the dye laser. Therefore it would not have been possible to establish the free-photon limit using a doped crystal and the dye laser. The Ti:Sa laser has a much wider tuning range when multiple mirror sets are used; it was used in this scan to obtain an adequate free-photon limit.

To get data from the impurity peak, it is necessary to collect phase data from deep inside the main stop band. The graph shows that the previous scan lost the fringe pattern at a wavelength that corresponds to a transmitted intensity two orders of magnitude below the value outside the stop band. However, observing the transmission spectrum of the doped crystal shows that the impurity has its peak at just above 10^{-2} relative intensity. Hence it would not have been possible to observe the phase change from the impurity with the original interferometer setup. Figure 11 shows that the improved instrument, incorporating the attenuation wheels, is able to increase the dynamic range by at least one order of magnitude, making it possible to map out the effects of impurities.

By improving the overall quality of the colloidal crystals and hence reducing scatter in the phase data, one might gain more detailed insight into the microstructural properties of the impurities. The issue of whether the dopant particles occupy substitutional sites or rather form regions of ordered alloy is an important one. A more rigid colloidal crystal, possibly with a solidified support matrix for the polystyrene microspheres,³⁵ will be helpful in addressing this issue.

6. SUMMARY

In summary, the feasibility of measuring photonic band structure in pure and doped colloidal crystals by interferometry has been demonstrated. This work demonstrates significant improvement of our earlier instrument in wavelength range and dynamic range for phase measurements. More accurate modeling of the nonphotonic phase shift has been incorporated as well. Preliminary data from impurity crystals demonstrate the feasibility of observing details of impurity states in photonic crystals by interferometry.

ACKNOWLEDGMENTS

We thank İ. İnanc Tarhan and Martin P. Zinkin for aid and previous work. We also acknowledge helpful discussions with Ranjit D. Pradhan. This research was supported by National Science Foundation grant DMR-9510460.

REFERENCES

1. E. Yablonovitch, "Inhibited spontaneous emission in solid-state physics and electronics," *Phys. Rev. Lett.* **58**, 2059 (1987).
2. S. John, "Strong localization of photons in certain disordered dielectric superlattices," *Phys. Rev. Lett.* **58**, 2486 (1987).
3. E. Yablonovitch, "Photonic bandgap structures," *J. Opt. Soc. Am. B* **10**, 283 (1993).
4. E. Yablonovitch, "Photonic band-gap crystals," *J. Phys. Condens. Matter* **5**, 2443 (1993).
5. E. Yablonovitch, "Photonic crystals," *J. Mod. Opt.* **41**, 173 (1994).
6. W. Robertson, G. Arjavalingam, R. D. Meade, K. D. Brommer, A. M. Rappe, and J. D. Joannopoulos, "Measurement of photonic band structure in a two-dimensional periodic dielectric array," *Phys. Rev. Lett.* **68**, 2023 (1992).
7. T. F. Krauss, R. M. De La Rue, and S. Brand, "Two-dimensional photonic bandgap structures operating at near-infrared wavelengths," *Nature (London)* **383**, 699 (1996).
8. U. Grüning, V. Lehmann, S. Ottow, and K. Busch, "Macroporous silicon with a complete two-dimensional photonic band gap centered at 5 μm ," *Appl. Phys. Lett.* **68**, 747 (1996).
9. A. Mekis, J. C. Chen, I. Kurland, S. Fan, P. R. Villeneuve, and J. D. Joannopoulos, "High transmission through sharp bends in photonic crystal waveguides," *Phys. Rev. Lett.* **77**, 3787 (1996).
10. J. D. Joannopoulos, P. R. Villeneuve, and S. Fan, "Photonic crystals: putting a new twist on light," *Nature (London)* **386**, 143 (1997).
11. P. R. Villeneuve, S. Fan, J. D. Joannopoulos, K.-Y. Lim, G. S. Petrich, L. A. Kolodziejski, and R. Reif, "Air-bridge microcavities," *Appl. Phys. Lett.* **67**, 167 (1995).
12. J. S. Foresi, P. R. Villeneuve, J. Ferrera, E. R. Thoen, G. Steinmeyer, S. Fan, J. D. Joannopoulos, L. C. Kimerling, H. I. Smith, and E. P. Ippen, "Photonic-bandgap microcavities in optical waveguides," *Nature (London)* **390**, 143 (1997).
13. C. C. Cheng and A. Scherer, "Fabrication of photonic bandgap crystals," *J. Vac. Sci. Technol.* **13**, 2696 (1995).
14. C. C. Cheng, V. Arbet-Engels, A. Scherer, and E. Yablonovitch, "Nanofabricated three dimensional photonic crystal operating at optical wavelengths," *Phys. Scr.* **T68**, 17 (1996).
15. K. M. Ho, C. T. Chan, C. M. Soukoulis, R. Biswas, and M. Sigalas, "Photonic band gaps in three dimensions: new layer-by-layer periodic structures," *Solid State Commun.* **89**, 413 (1994).
16. S. Fan, P. R. Villeneuve, R. D. Meade, and J. D. Joannopoulos, "Design of three-dimensional photonic crystals at sub-micron length scales," *Appl. Phys. Lett.* **65**, 1466 (1994).
17. P. Pieranski, "Colloidal crystals," *Contemp. Phys.* **24**, 25 (1983).
18. N. A. Clark, A. J. Hurd, and B. J. Ackerson, "Single colloidal crystals," *Nature (London)* **281**, 57 (1979).
19. İ. İ. Tarhan and G. H. Watson, "Photonic band structure of *fcc* colloidal crystals," *Phys. Rev. Lett.* **76**, 315 (1996).
20. R. D. Pradhan, J. A. Bloodgood, and G. H. Watson, "Photonic band structure of *bcc* colloidal crystals," *Phys. Rev. B* **55**, 9503 (1997).
21. W. L. Vos, R. Sprik, A. vanBlaaderen, A. Imhof, A. Lagendijk, and G. H. Wegdam, "Strong effects of photonic band structures on the diffraction of colloidal crystals," *Phys. Rev. B* **53**, 16231 (1996).
22. R. Biswas, M. M. Sigalas, G. Subramania, and K.-M. Ho, "Photonic band gaps in colloidal crystals," *Phys. Rev. B* **57**, 3701 (1998).
23. Duke Scientific Corporation, 2463 Faber Place, Palo Alto, Calif. 94303.
24. P. Pieranski, E. Dubois-Violette, F. Rothen, and L. Strzelecki, "Geometry of Kossel lines in colloidal crystals," *J. Phys. (France)* **42**, 53 (1981).
25. J. B. Bateman, E. J. Weneck, and D. C. Eshler, "Determination of particle size and concentration from spectrophotometric transmission," *J. Colloid Sci.* **14**, 308 (1959).
26. R. H. Boundy and R. F. Boyer, *Styrene: Its Polymers, Copolymers and Derivatives* (Hafner, New York, 1965).
27. I. Thormahlen, J. Straub, and U. Grigul, "Refractive index of water and its dependence on wavelength, temperature and density," *J. Phys. Chem. Ref. Data* **14**, 933 (1985).
28. İ. İ. Tarhan, M. P. Zinkin, and G. H. Watson, "Interferometric technique for the measurement of photonic band structure in colloidal crystals," *Opt. Lett.* **20**, 1571 (1995).
29. P. Hariharan, "Modified Mach-Zehnder interferometer," *Appl. Opt.* **8**, 1925 (1969).
30. Omega Optical Inc., P.O. Box 573, Brattleboro, Vermont 05302.
31. İ. İ. Tarhan, "Investigation of optical photonic band structure in *fcc* colloidal crystals," Ph.D. dissertation (U. Delaware, Newark, Del., 1996).
32. İ. İ. Tarhan and G. H. Watson, "Analytical expression for the optimized stop bands of *fcc* photonic crystals in the scalar-wave approximation," *Phys. Rev. B* **54**, 7593 (1996).
33. E. Yablonovitch, T. J. Gmitter, R. D. Meade, A. M. Rappe, K. D. Brommer, and J. D. Joannopoulos, "Donor and acceptor modes in photonic band structure," *Phys. Rev. Lett.* **67**, 3380 (1991).
34. R. D. Pradhan, İ. İ. Tarhan, and G. H. Watson, "Impurity modes in the optical stop bands of doped colloidal crystals," *Phys. Rev. B* **54**, 13721 (1996).
35. S. A. Asher, J. Holtz, L. Liu, and Z. Wu, "Self-assembly motif for creating submicron periodic materials. Polymerized crystalline colloidal arrays," *J. Am. Chem. Soc.* **116**, 4997 (1994).